● *Original Contribution*

COMPARISON OF SOUND TOUCH ELASTOGRAPHY, SHEAR WAVE ELASTOGRAPHY AND VIBRATION-CONTROLLED TRANSIENT ELASTOGRAPHY IN CHRONIC LIVER DISEASE ASSESSMENT USING LIVER BIOPSY AS THE "REFERENCE STANDARD"

ILIAS GATOS,*,[†] PETROS DRAZINOS,* SPYROS YARMENITIS,*
IOANNIS THEOTOKAS,* and PAVLOS S. ZOUMPOULIS*

* Diagnostic Echotomography SA, Kifissia, Greece; and [†] Department of Medical Physics, School of Medicine, University of Patras, Rion, Greece

Abstract—Chronic liver disease (CLD) is currently a major cause of death. Ultrasound elastography (USE) is an imaging method that has been developed for CLD assessment. Our aim in the study described here was to evaluate and compare a new commercial variant of USE, sound touch elastography (STE), with already established USE methods, shear wave elastography (SWE) and vibration-controlled transient elastography (VCTE), using liver biopsy as the "reference standard." For our study, 139 consecutive patients underwent standard liver STE, SWE and VCTE examinations with the corresponding ultrasound devices. A receiver operator characteristic (ROC) curve analysis was performed on the stiffness values measured with each method. ROC analysis revealed, for SWE, STE and VCTE, areas under the ROC curve of 0.9397, 0.9224 and 0.9348 for fibrosis stage (F), $F \geq F1$; 0.9481, 0.9346 and 0.9415 for $F \geq F2$; 0.9623, 0.9591 and 0.9631 for $F \geq F3$; and 0.9581, 0.9541 and 0.9632 for $F = F4$, respectively. In conclusion, STE performs similarly to SWE and VCTE in CLD stage differentiation. (E-mail: p.zoumpoulis@echomed.gr)   © 2020 The Author(s). Published by Elsevier Inc. on behalf of World Federation for Ultrasound in Medicine & Biology. This is an open access article under the CC BY-NC-ND license. (http://creativecommons.org/licenses/by-nc-nd/4.0/).

Key Words: Chronic liver disease, Fibrosis, Sound touch elastography, Shear wave elastography, Vibration-controlled transient elastography.

INTRODUCTION

Chronic liver disease (CLD) is responsible for approximately 2 million deaths per year worldwide, of which 1 million are owing to complications of cirrhosis and 1 million are owing to viral hepatitis and hepatocellular carcinoma (HCC). Cirrhosis and liver cancer combined account for 3.5% of all deaths worldwide (Asrani et al. 2019). As most causes of CLD are preventable, there is an important opportunity to improve public health by improving the diagnostic accuracy of CLD assessment.

CLD may be caused by viruses, mainly hepatitis B virus (HBV) or hepatitis C virus (HCV), and by excessive alcohol consumption. Bad nutrition habits can lead to non-alcoholic fatty liver disease (NAFLD) and steatohepatitis (NASH), which are the most frequent types of CLD in Western countries. Rarer CLD subtypes include autoimmune hepatitis (AIH); primary biliary cholangitis (PBC), previously referred as primary biliary cirrhosis; secondary biliary cholangitis; primary sclerosing cholangitis; and Wilson's disease (Friedman and Martin 2017).

CLD causes constant liver tissue injury and inflammation that leads to the development of fibrosis and, at the end stage of the disease, cirrhosis. Cirrhosis leads to liver failure and, in many cases, to HCC development and death. Evidence provided by recent published data indicates that successful treatment of CLD may result in fibrosis regression (Parola and Pinzani 2019). It is therefore important to monitor progress or regression of hepatic fibrosis to validate the effectiveness of different therapeutic protocols.

Address correspondence to: Pavlos S. Zoumpoulis, Diagnostic Echotomography SA, 317C Kifisias Avenue, 14561 Kifissia, Greece. E-mail: p.zoumpoulis@echomed.gr

To recommend appropriate patient management, the etiology, stage and activity of CLD should be diagnosed accurately. Liver biopsy (LB) is still considered the "reference standard" for CLD assessment. LB is the only diagnostic method that can identify certain CLD subtypes, such as NASH and autoimmune hepatitis, and determine CLD activity. Regarding CLD staging, LB diagnosis involves the use of fibrosis severity classification systems such as the Ishak and Metavir. The Metavir classification system, the most widely used, is a five fibrosis stage (F) scale, ranging from F0−F4 (F0 = no fibrosis, F1 = mild fibrosis, F2 = significant fibrosis, F3 = severe fibrosis, F4 = cirrhosis) (Goodman 2007). Although LB serves as reference standard, it has serious limitations. It is invasive and expensive, and nearly 30% of patients suffer post-procedural side effects, such as substantial pain, pneumothorax, bleeding, infection, septicemia, biloma, hemobilia and accidental injury to adjacent structures and biliary peritonitis. In rare cases, even death may occur (<1%) (Gilmore et al. 1995; Carey and Carey 2010). Furthermore, liver fibrosis is not uniformly distributed, and as the needle biopsy provides a very small volume of tissue (1/50,000th of the total mass of the liver), biopsy sample variability is common (Carey and Carey 2010).

The need to overcome LB limitations has led to the employment of a series of non-invasive approaches to CLD assessment. These include blood serum markers (BSMs) and various imaging modalities, such as computed tomography (CT), magnetic resonance imaging (MRI) and ultrasound (US). BSMs and CT perform adequately in estimating significant fibrosis (F ≥ F2) and cirrhosis (F4), but fail in assessing early stages of the disease (Romero-Gómez et al. 2008; Carey and Carey 2010; Martínez et al. 2011; Frulio and Trillaud 2013). US B-mode, on the other hand, recognizes only diffuse abnormalities (Sanford et al. 1985) and the absence of cirrhosis (Harbin et al. 1980; Giorgio et al. 1986).

Regarding MRI, a new but very promising contemporary imaging technique, magnetic resonance elastography (MRE), exhibits great accuracy at all stages. MRE has also exhibited fibrosis heterogenicity through the liver as it has provided significantly different stiffness values in different liver segments (Akkaya et al. 2018). Although MRE is very accurate, it is costly and requires further validation (Huwart et al. 2008; Carey and Carey 2010; Akkaya et al. 2018).

Ultrasound elastography (USE) is a new US-based method introduced during the last two decades that contributes to CLD diagnosis by correlating fibrosis to liver tissue stiffness. Many USE variants, based on different technologies, are commercially available and include vibration-controlled transient elastography (VCTE), widely known as Fibroscan, acoustic radiation force impulse (ARFI) elastography, real-time elastography (RTE) and shear wave elastography (SWE). Most of these methods provide quantitative stiffness measurements for CLD stage estimation. All clinical studies employing USE are based on optimum, usually LB-validated, stiffness cutoff values that correspond to fibrosis stages (Ferraioli et al. 2012, 2015; Bamber et al. 2013; Cosgrove et al. 2013; Bota et al. 2013, 2015; Frulio and Trillaud 2013; Deffieux et al. 2015; Gerber et al. 2015; Kobayashi et al. 2015; Li [Mindray Bio-Medical Electronics Co. Ltd] 2015; Dietrich et al. 2017; Herrmann et al. 2018; Ren et al. 2018).

VCTE carried out with the Fibroscan US device (Echosens, Paris, France) is the first and most validated technique utilized for liver fibrosis estimation. VCTE performs well on advanced fibrosis stages (F ≥ F2, F ≥ F3, F = F4), and its mean diagnostic accuracy has an area under the curve (AUC) value of 0.85, with an average sensitivity of 0.78 and specificity of 0.79 (Talwalkar et al. 2007; Vizzutti et al. 2009; Tsochatzis et al. 2011; Bota et al. 2013; Chung et al. 2013; Frulio and Trillaud 2013). Various studies have reported good intra- and inter-observer agreement for VCTE (Talwalkar et al. 2007; Vizzutti et al. 2009). Although accurate in estimation of advanced fibrosis stages, VCTE suffers from overlap between optimum fibrosis stage cutoff values in several studies. Furthermore, VCTE is less accurate in assessing early stages of the disease. Another elastography technique, acoustic radiation force impulse (ARFI) elastography, presented by SIEMENS, is equivalent in performance to VCTE (mean AUC value: 0.85), with similar limitations regarding the stiffness optimum cutoff overlap (Bota et al. 2013; Chung et al. 2013). Similarly, Hitachi's elastographic approach, RTE, reaches a mean AUC of 0.85, average sensitivity of 0.83 and specificity of 0.77 for significant fibrosis (F ≥ F2) (Chung et al. 2013; Bota et al. 2015; Kobayashi et al. 2015). According to meta-analyses, RTE is useful only in visualizing tissue stiffness differences subjectively, but does not provide a stiffness measurement that would result in quantified CLD stage information (Bota et al. 2015; Kobayashi et al. 2015). Supersonic Imagine (Aix-en-Provence, France) is one of the manufacturers that provide real-time 2-D elasticity imaging, as well as stiffness quantification. Other variants of 2-D-SWE are provided by other commercial alternatives. SWE, therefore, contrary to other methods that do not apply 2-D elastographic imaging, provides the examiner with an opportunity to choose a region of interest. Although it has high classification rates (mean AUC values of 0.81 for fibrosis stage (F) ≥ F1 and 0.86 for F ≥ F2), SWE has several limitations such as stiffness cutoff threshold variability between different studies and challenges in recognizing and avoiding artifacts and noise areas, as

well as uncertainties in the selection of the optimum quantification region (Ferraioli et al. 2012, 2015; Bamber et al. 2013; Sporea et al. 2014; Gerber et al. 2015; Cosgrove et al. 2013; Bota et al. 2015; Deffieux et al. 2015; Dietrich et al. 2017; Sigrist et al. 2017; Herrmann et al. 2018).

Motivated by 2-D elastographic imaging's strengths and its popularity among radiologists, other manufacturers, such as Toshiba, GE, Philips and Mindray, have developed and incorporated similar techniques into their US systems (Dietrich et al. 2017). These techniques differ with respect to the details of each method and require validation to be considered established. Toshiba, Philips and Mindray seem to have implemented methods similar to Siemens's conventional ARFI pushing technique. A recent study by Gress et al. (2019) on healthy volunteers at various measurement depths revealed that different SWE technological implementations, such as the Siemens Acuson S3000, GE LOGIQ E9, Philips EPIQ7 and Toshiba Aplio 500 (Version 6), are equivalent in performance. Mindray employs a new technology to provide real-time stiffness imaging. An acoustic radiation force-based US pulse is used to generate shear waves.

Subsequently, the shear wave propagation is tracked by the system to detect and record the induced tissue displacements. The shear wave propagation speed and elastic modulus are then calculated in different positions to form a full elasticity image. For this procedure to be possible in real time, Ultra-wide Beam Tracking Imaging signal receiving technology is employed. This technology achieves shear wave signal sampling up to 10 kHz per frame within areas from 0.2−40 mm wide in one shot. The necessary data are captured in less than several tenths of a millisecond (Li [Mindray Bio-Medical Electronics Co. Ltd] 2015). This technique employed on the Resona 7 system is commercially known as sound touch elastography (STE). To date, the number of clinical studies that have reported on and evaluated STE performance on various organs and pathologies is limited (Dong et al. 2019; Zhang et al. 2018); there are few published studies concerning STE performance in CLD fibrosis stage evaluation (Li et al. 2018; Ren et al. 2018). Li et al. (2018) compared the performance of STE and MRE on 33 rabbit livers and obtained similar results for the two modalities. In a recent study, Ren et al. (2018) compared the diagnostic performance of Mindray's STE and sound
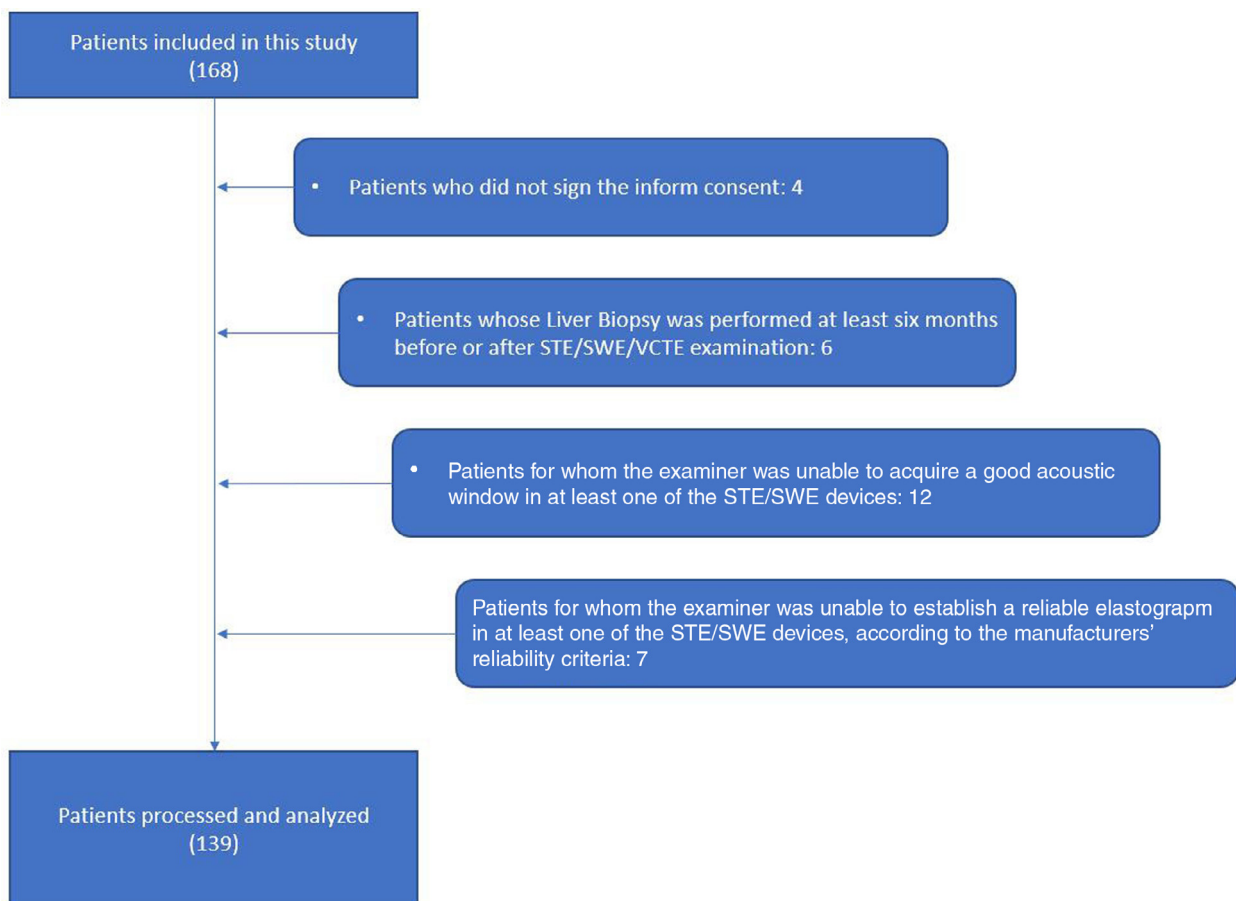

Fig. 1. Flowchart of patient eligibility process.

touch quantification methods, along with VCTE, in 158 patients with HBV obtaining accuracies of 87.0, 65.1 and 64.8, respectively, for F $\geq$ F2 fibrosis stage differentiation.

We decided to perform this study, first, because STE introduces a new technological approach in shear wave elastographic imaging that, because of the different physics principles involved, may be more accurate in stiffness estimation compared with other elastographic approaches. Furthermore, there is a lack of information on STE performance in CLD diagnosis, and access to multiple competitive US systems as well as significant CLD patient examination flow provided us with an opportunity to compare the performance of STE, SWE and VCTE using LB as the reference standard.

METHODS

Clinical data

Between September 2017 and January 2019, 168 patients (91 men and 75 women) were processed for the purpose of this prospective study. Their mean age was 60 $\pm$ 14.27 and their ages varied between 22 and 89. Twenty-nine patients were excluded from the study for having at least one of the following exclusion criteria: 4 did not sign the informed consent form, 6 had undergone a LB more than 6 mo before or after their SWE/STE/ VCTE examination; for 12 patients, the examiner was unable to acquire a good acoustic window with at least one of the devices; and for 7 patients, the examiner was unable to acquire a reliable elastogram with at least one of the STE/SWE devices, using the manufacturers' reliability criteria described in more detail below. Figure 1 is a flowchart of the exclusion process. Of the remaining 139 patients (80 men and 59 women) with a mean age of 60.67 y, who were examined and analyzed, 28 were normal (F0) and 111 had CLD (46 F1, 12 F2, 21 F3 and 32 F4). In detail, 20 had HBV, 22 HCV, 14 alcoholic liver disease, 29 NAFLD, 18 AIH, 6 PBC and 30 with other CLD etiology. All clinical and histologic data from this study are summarized in Table 1. Normal patients (F0) comprised healthy volunteers of any age and sex with a clear clinical history regarding CLD absence, normal biochemical markers and normal liver findings in the US examination. Their VCTE and SWE measurements were within the normal stiffness value range (4.4−5.5 kPa for both TE and SWE/STE methods) provided by the European Federation of Societies for Ultrasound in Medicine and Biology (EFSUMB) guidelines (Dietrich et al. 2017). Patients with CLD (F1−F4), were validated by liver biopsy and histologic examination by a senior histopathologist with extensive experience in liver histology, who was unaware of the SWE, STE and VCTE measurements. The SWE, STE and VCTE examinations

Table 1. Baseline characteristics of patients who participated in the study

Age (y)	60.67 (22−89)
Sex	
Male	80 (57.55%)
Female	59 (42.45%)
Body mass index (kg/m^2)	26.72 $\pm$ 5.77
Diagnosis	
Chronic hepatitis B	20 (14.39%)
Chronic hepatitis C	22 (15.83%)
Alcoholic liver disease	14 (10.07%)
NAFLD	29 (20.86%)
Autoimmune hepatitis	18 (12.95%)
Primary biliary cholangitis	6 (4.32%)
Other	30 (21.58%)
Fibrosis stage (METAVIR)	
F0	28 (20.14%)
F1	46 (33.09%)
F2	12 (8.63%)
F3	21 (15.11%)
F4	32 (23.02%)

NAFLD = non-alcoholic fatty liver disease.

were performed on the right lobe of each patient's liver according to EFSUMB guidelines (Dietrich et al. 2017). The World Federation for Ultrasound in Medicine and Biology (WFUMB) has also published recommendations regarding the use and performance of the various elastographic techniques. With respect to the procedure for VCTE and SWE/STE examinations, both EFSUMB and WFUMB guidelines concur on examination procedure details, such as number of measurements for each technique and patient fasting before examination (Ferraioli et al. 2015, 2018; Dietrich et al. 2017). The potential risk of examiners being biased by dependence of the STE/ SWE measurements on the order of examinations was limited by randomly setting the order of the examinations with the two US systems. Although a lack of registration between LB samples and elastographic measurements exists, LB is considered the reference standard because a uniform distribution of fibrosis throughout the liver is assumed in all imaging studies correlating LB and stiffness measurements. This study was conducted in accordance with the ethical guidelines of the Helsinki Declaration and was approved by our institutional review board; written informed consent was obtained from all patients participating in the study.

Exclusion criteria

The criteria for exclusion from the study included unwillingness to participate in the study or to provide informed consent, absence of LB or LB performed more than 6 mo before or after the SWE/STE/VCTE examination, absence of either SWE/STE/VCTE examinations or an time interval longer than 6 mo between them and evidence of HCC. Finally, inability to obtain a clear acoustic window during the SWE/STE examination and absence

of acceptable reliability criteria, provided by the manufacturers of the systems, were also exclusion criteria.

Examination protocol

A regular B-mode and color/power Doppler US abdominal examination was performed on each patient by two expert radiologists (EFSUMB experience level 3) having at least 10 y of experience in VCTE and SWE and 1 y of experience in STE in the liver. The SWE examination was performed on the Aixplorer US system (Supersonic Imagine, Aix-en-Provence, France) with an SC6-1 curvilinear transducer, and STE examination was performed on the Resona 7 US system, using a convex SC5-1 U transducer. The SWE and STE examinations were performed on the same day for each patient by the two examiners. VCTE examination was performed in two medical centers and differed no more than 1 mo in time from the SWE/STE examinations. The VCTE examination results were sent to our medical center where the median of 10 measurements and inter-quartile range (IQR) were stored for processing. For the SWE/STE examination, after establishing a good acoustic window, the examiner activated the elastography mode and waited for the elastogram to be stable for five consecutive frames To ensure the quality of measurements with both SWE and STE, the reliability (RLB) map and motion stability (M-STB) index for the Resona 7's STE and the stability index (SI) for Supersonic Imagine's SWE were used (Fig. 2), according to the corresponding manufacturer's guidelines. In detail, Resona 7 offers two reliability indexes, the M-STB index and the RLB map. The M-STB helps to monitor the degree of motion interference, which may be induced by patient respiration or movement of the transducer in real time. A low star number (<4) indicates the motion interference is high, and a high star number (≥ 4) indicates the motion interference is low or does not exist. To assist the user, the low star number is associated with the color orange, and the high star number with the color green. An M-STB index that is green for several consecutive frames indicates that the shear wave elastogram is stable. The RLB map is related to the STE shear wave intensity and indicates the areas in which a reliable measurement is possible with the color green; areas associated with unreliable measurements are purple colored. Each STE measurement was taken by avoiding purple areas on the RLB map and ensuring at least four green stars in the five-star stability index.

The Aixplorer system offers a measurement stability index, which is derived from the spatial and temporal stiffness stability of the circular region of interest (ROI) (Qbox), used to perform the SWE measurement. Each SWE measurement was taken at a stability index $>90\%$. The median value of 5 SWE/STE measurements (derived from 5 different SWE/STE frames) and of 10 VCTE measurements was calculated and saved for further analysis. The number of measurements for each technique used in this study is recommended by both EFSUMB and WFUMB guidelines (Ferraioli et al. 2015, 2018; Dietrich et al. 2017). An IQR to median ratio (IQR/M) $<30\%$ ensured measurement reliability for all elastography systems used in this study. All measurements in all devices used in this study were calculated in kilopascals using Young's modulus.

Statistical analysis

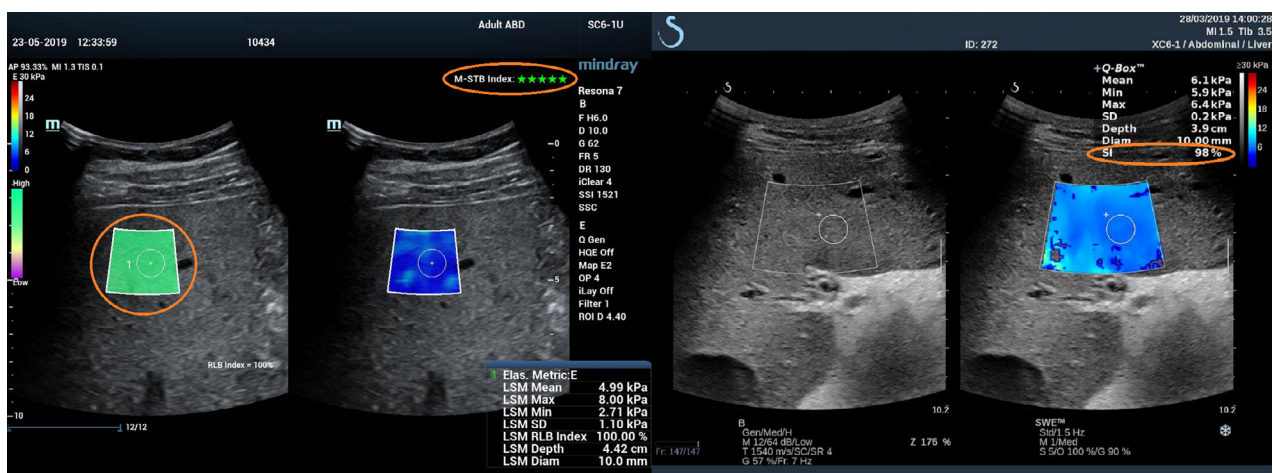The SWE/STE and VCTE measurements were archived, and a receiver operating characteristic (ROC)

Fig. 2. Indicative images of sound touch elastography and shear wave elastography methods with their reliability indices marked in orange ellipses. Left: Sound touch elastography with reliability map and motion stability index. Right: Shear wave elastography with stability index.

analysis was performed (Lasko et al. 2005) using LB fibrosis stages (Metavir) as the reference standard, to calculate the optimum cutoff values for CLD stage differentiation. Optimum cutoffs are defined as stiffness values that correspond to points on the ROC curve with minimum distance from the point (0,1). Additionally, intra-observer variability was assessed for each examiner, and inter-observer variability was assessed for each patient, using the intra-correlation coefficient (ICC) for pairs of measurements made by the two examiners. Inter-device variability was calculated for each patient and the first examiner for each pair of systems (SWE−VCTE, STE−VCTE and SWE−STE).

RESULTS

The data collected from the US examinations were used to perform an ROC analysis to calculate metrics such as sensitivity, specificity, area under the ROC curve (AUC), accuracy and, therefore, the best cutoff values for each technique (SWE, STE, VCTE). For the ROC analysis, LB was used as the reference standard. SWE, STE and VCTE measurements were also used to assess inter-observer, intra-observer and inter-device variability *via* the ICC, Pearson correlation and Bland−Altman plots (Bland and Altman 1999).

ROC analysis

ROC analysis was performed to calculate the optimum cutoff values for the three techniques (STE, SWE, VCTE) for the following binary classifications of CLD staging: F ≥ F1, F ≥ F2, F ≥ F3 and F = F4. In the case of F ≥ F1, VCTE achieved the highest accuracy of the three techniques with a value of 0.8849. SWE and STE achieved accuracies of 0.8633 and 0.8417, respectively. The highest AUC value achieved was 0.9397 by SWE, while VCTE had an AUC a value of 0.9348. STE had an AUC value of 0.9224. The cutoff values for VCTE, SWE and STE are 6.2, 7.05 and 7.15 kPa, respectively. In the classification of F ≥ F2, SWE and VCTE achieved the highest accuracy, which was the same for both techniques, 0.8921. STE achieved a value of 0.8633. The AUC value of SWE was 0.9481. VCTE and STE had AUC values of 0.9415 and 0.9346, respectively. The threshold values for VCTE, SWE and STE were 7.6, 8.3 and 8.0 kPa, respectively. In the case of F ≥ F3, STE had the highest accuracy of the three techniques, 0.9424. VCTE followed with an accuracy of 0.9281, and SWE, with 0.9065. VCTE achieved an AUC value of 0.9631 and was followed by SWE and STE with values of 0.9623 and 0.9591, respectively. The threshold values for this classification for VCTE, SWE and STE were 8.8, 8.7 and 9.05 kPa, respectively. In the last classification of F = F4, VCTE had the highest accuracy, 0.9281. SWE

achieved an accuracy of 0.9209, and STE, 0.9137. The AUC values of VCTE, SWE and STE were 0.9632, 0.9581 and 0.9541, respectively. The cutoff values for VCTE, SWE and STE were 10.6, 10.5 and 11.05 kPa. AUC, accuracy and threshold values for each technique, along sensitivity, specificity and balanced accuracy, are outlined in detail in Tables 2, 3, 4 and 5 and Figure 3.

Inter- and intra-observer variability

The results of the inter-observer variability analysis are outlined in Table 6 and illustrated in Figure 4. SWE had a mean inter-observer variability of −0.52 (standard deviation [SD] = 2.54) kPa, and STE, a mean value of 0.1 (SD = 1.57) kPa. The ICC was 0.9610 for SWE and 0.98 for STE. The results for intra-observer variability analysis are outlined in detail in Tables 7 and 8. SWE had mean intra-observer variability values of −0.01 and

---

Table 2. ROC analysis results for F ≥ F1

Method	SWE	STE	VCTE
Area under ROC curve	0.9397	0.9224	0.9348
Sensitivity	0.8627	0.8431	0.9216
Specificity	0.8649	0.8378	0.7838
Balanced accuracy	0.8638	0.8405	0.8527
Accuracy	0.8633	0.8417	0.8849
Threshold, cutoff value (kPa)	7.05	7.15	6.2

ROC = receiver operating characteristic; STE = sound touch elastography; SWE = shear wave elastography; VCTE = vibration-controlled transient elastography.

Table 3. ROC analysis results for F ≥ F2

Method	SWE	STE	VCTE
Area under ROC curve	0.9481	0.9346	0.9415
Sensitivity	0.8533	0.8533	0.8800
Specificity	0.9375	0.8750	0.9063
Balanced Accuracy	0.8954	0.8642	0.8931
Accuracy	0.8921	0.8633	0.8921
Threshold, cutoff value (kPa)	8.3	8.0	7.6

ROC = receiver operating characteristic; STE = sound touch elastography; SWE = shear wave elastography; VCTE = vibration-controlled transient elastography.

Table 4. ROC analysis results for F ≥ F3

Method	SWE	STE	VCTE
Area under ROC curve	0.9623	0.9591	0.9631
Sensitivity	0.9298	0.9474	0.9123
Specificity	0.8902	0.9390	0.9390
Balanced accuracy	0.9100	0.9432	0.9257
Accuracy	0.9065	0.9424	0.9281
Threshold, cutoff value (kPa)	8.7	9.05	8.8

ROC = receiver operating characteristic; STE = sound touch elastography; SWE = shear wave elastography; VCTE = vibration-controlled transient elastography.

Table 5. ROC analysis results for F = F4

Method	SWE	STE	VCTE
Area under ROC curve	0.9581	0.9541	0.9632
Sensitivity	0.9286	0.9286	0.9286
Specificity	0.9175	0.9072	0.9278
Balanced accuracy	0.9230	0.9179	0.9282
Accuracy	0.9209	0.9137	0.9281
Threshold, cutoff value (kPa)	10.5	11.05	10.6

ROC = receiver operating characteristic; STE = sound touch elastography; SWE = shear wave elastography; VCTE = vibration-controlled transient elastography.

−0.02 for the first and second examiners, respectively. STE had values of 0.56 and −0.27 for the first and second examiners, respectively. The SD of SWE variability was 0.73 for the first examiner and 2.6 for the second examiner. The SD of STE variability was 1.33 for the first examiner and 2.31 for the second examiner. The ICC for SWE was 0.99 for the first examiner and 0.97 for the second examiner. For STE, the ICC was 0.95 for the first examiner and 0.97 for the second examiner.

Inter-device variability

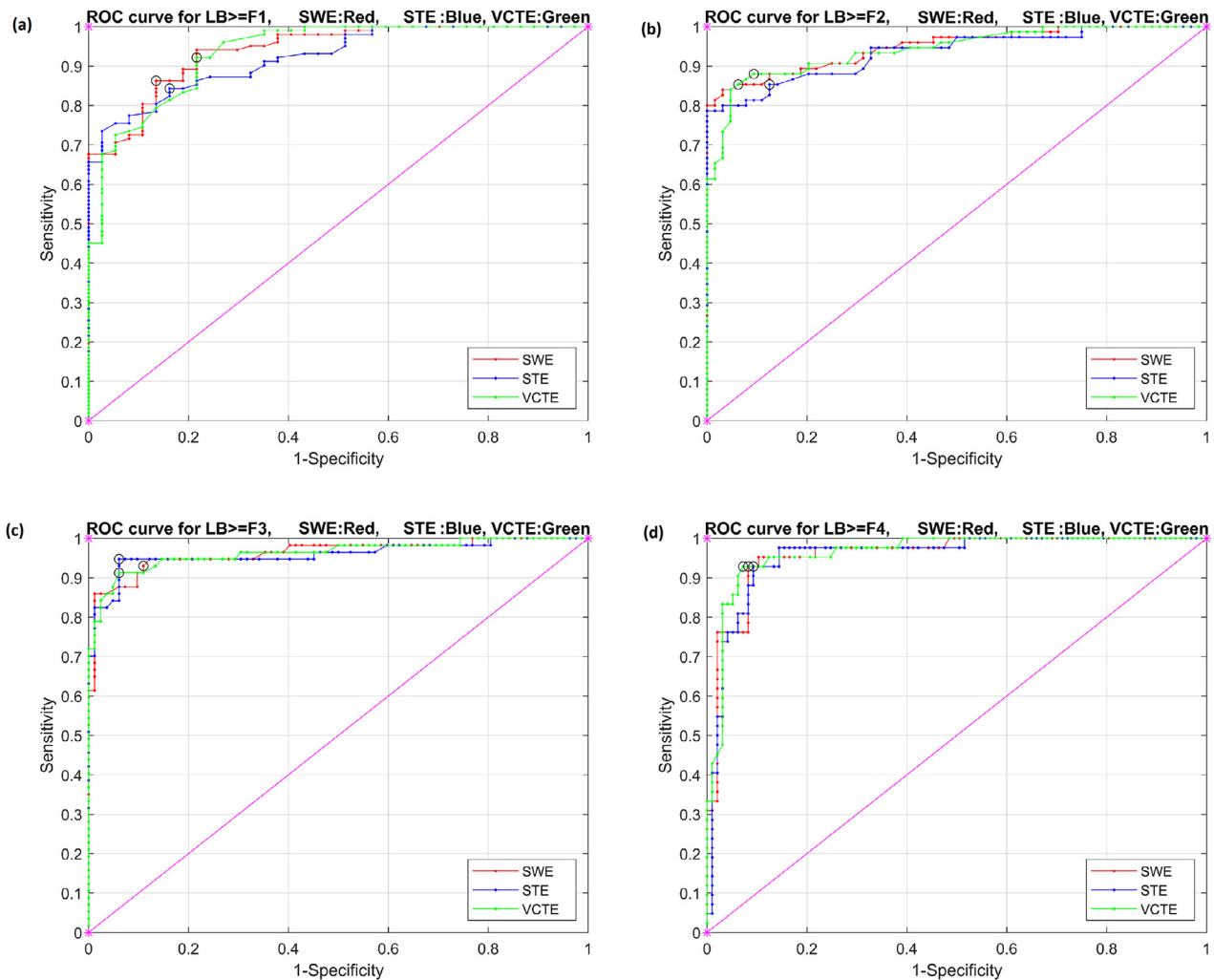Inter-device variability analysis was performed on pairs of US devices produced by different manufacturers,

Fig. 3. Receiver operating characteristic (ROC) analysis for shear wave elastography (SWE, *red*), sound touch elastography (STE, *blue*) and vibration-controlled transient elastography (VCTE, *green*) with optimum cutoff points marked in *black circles* for F ≥ F1 (a), F ≥ F2 (b), F ≥ F3 (c) and F = F4 (d). LB = liver biopsy.

Table 6. Inter-observer variability-related results for SWE and STE measurements*

Inter-observer variability (observer 1, observer 2)		
Method	SWE	STE
Mean($M_1 - M_2$) (kPa)	−0.52	0.1
SD($M_1 - M_2$) (kPa)	2.54	1.57
Intra-class correlation coefficient	0.9610	0.98
Pearson's correlation coefficient	0.99	0.99
Slope of least squares	1.2	0.95

M_1 = measurement from radiologist 1; M_2 = measurement from radiologist 2; SD = standard deviation; SWE = shear wave elastography; STE = sound touch elastography.

* Mean($M_1 - M_2$) and SD($M_1 - M_2$) are the mean and SD values of the subtraction of measurements of observer 1 and observer 2 for each patient on each device.

Table 7. Intra-observer variability-related results for SWE and STE measurements*

Intra-observer variability (observer 1)		
Method	SWE	STE
Mean ($M_1 - M_2$) (kPa)	−0.01	0.56
SD($M_1 - M_2$) (kPa)	0.73	1.33
Intra-class correlation coefficient	0.99	0.95
Pearson's correlation coefficient	1	0.99
Slope of least squares	0.99	0.89

M_1 = measurement 1 from radiologist 1; M_2 = measurement 2 from radiologist 1; SD = standard deviation; SWE = shear wave elastography; STE = sound touch elastography.

* Mean(M_1-M_2) and SD(M_1-M_2) are the mean and SD values of the subtraction of the two measurements of observer 1 on each device.
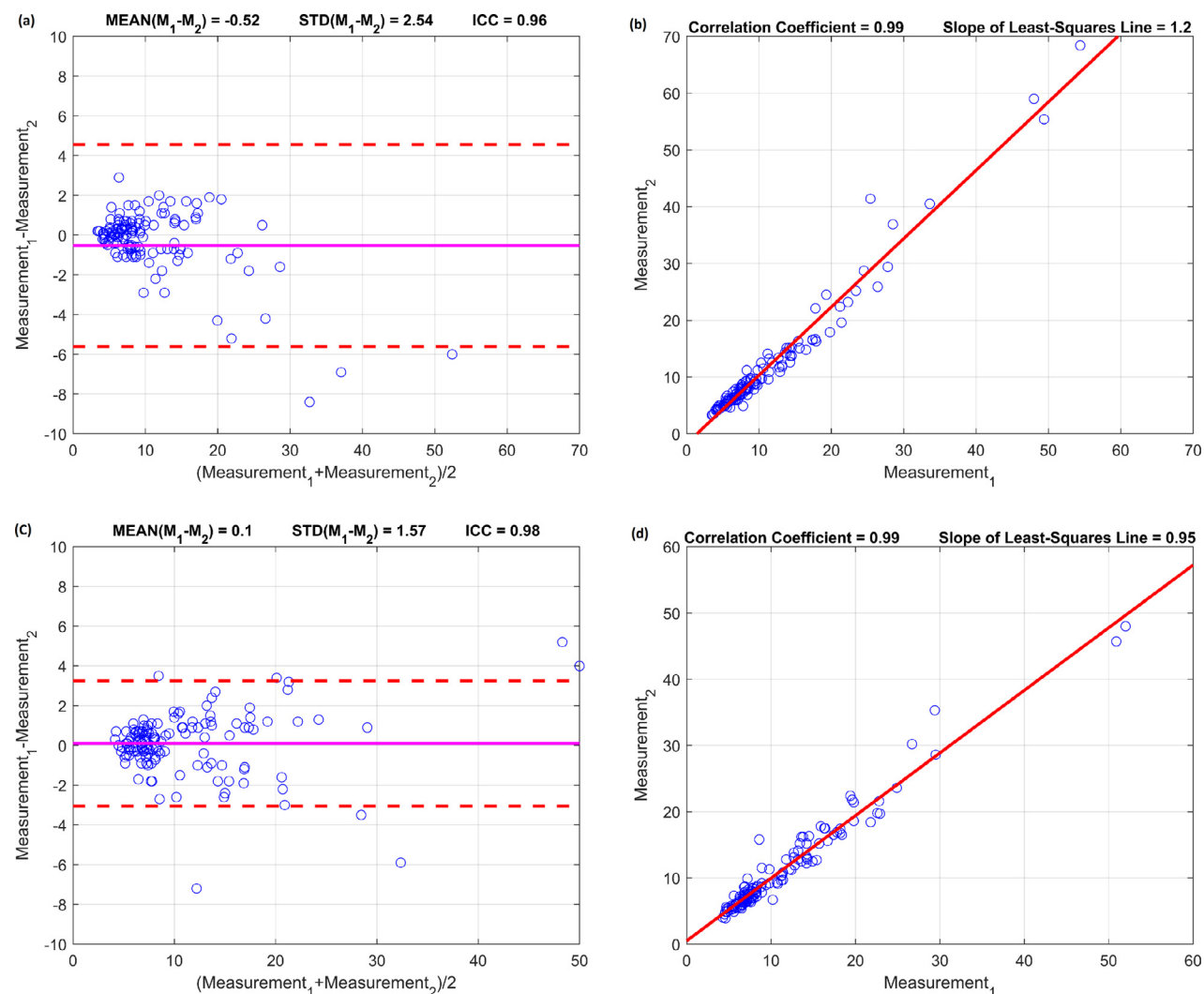

Fig. 4. (a,b) Shear wave elastography Bland−Altman (a) and least-squares line (b) plots. (c,d) Sound touch elastography Bland-Altman (c) and least-squares line (d) plots. Measurements were made to assess the inter-observer variability of each elastography method. ICC = intra-class correlation coefficient; STD = standard deviation.

Table 8. Intra-observer variability-related results for SWE and STE measurements*

	Intra-Observer variability (observer 2)	
Method	SWE	STE
Mean(M₁ − M₂) (kPa)	−0.02	−0.27
SD(M₁ − M₂) (kPa)	2.6	2.31
Intra-class correlation coefficient	0.97	0.97
Pearson's correlation coefficient	0.99	0.99
Slope of least squares	1.06	1.06

M_1 = measurement 1 from radiologist 2; M_2 = measurement 2 from radiologist 2; SD = standard deviation; SWE = shear wave elastography; STE = sound touch elastography.

* Mean(M_1-M_2) and SD(M_1-M_2) are the mean and SD values of the subtraction of the two measurements of observer 2 on each device.

each representing one of the three techniques (VCTE, SWE or STE). The mean inter-device variability of the SWE−VCTE pair was 0.32 kPa; that for the STE−VCTE pair, 0.3 kPa; and that for the SWE−STE pair, 0.02 kPa. The SDs of the three pairs SWE−VCTE, STE−VCTE and SWE−STE were 3.28, 3.81 and 3.35 kPa, and the ICC values were 0.92, 0.88 and 0.91, respectively. The results of the inter-device variability analysis are outlined in Table 9 and illustrated in Figure 5.

In Figure 6 are the stiffness values of each technique per fibrosis Metavir stage as measured in our study. The *box* indicates the IQR (second and third quartiles), the *black line* within the box indicates the median value, the *black whiskers* below and above the box indicate the first and fourth quartiles, respectively, and the black dots below or above the whiskers represent outliers.

DISCUSSION

In the study described here, STE, SWE and VCTE were compared with respect to their performance in

Table 9. Inter-device variability-related results for SWE-VCTE, STE-VCTE and SWE-STE measurements*

	Method pair		
	SWE−VCTE	STE−VCTE	SWE−STE
Mean(D₁ − D₂) (kPa)	0.32	0.3	0.02
SD(D₁ − D₂) (kPa)	3.28	3.81	3.35
Intra-class correlation coefficient	0.92	0.88	0.91
Pearson's correlation coefficient	0.97	0.96	0.97
Slope of least squares	0.92	1	0.81

D_1 = measurement from device 1; D_2 = measurement from device 2; SD = standard deviation; STE = sound touch elastography; SWE = shear wave elastography; VCTE = vibration-controlled transient elastography.

* Mean(D_1 − D_2) and SD(D_1 − D_2) are the mean and SD values of the subtraction of measurements in device 1 and device 2 for each patient from the same examiner.

CLD assessment. One hundred thirty-nine consecutive LB-validated patients were examined with all three methods, and ROC analysis was performed along with inter-observer and inter-device analyses. SWE, STE and VCTE achieved accuracies of 0.8633, 0.8417 and 0.8849 for F ≥ F1; 0.8921, 0.8633 and 0.8921 for F ≥ F2; 0.9065, 0.9424 and 0.9281 for F ≥ F3; and 0.9209, 0.9137 and 0.9281 for F = F4, respectively. These results indicate that all systems perform similarly in CLD diagnosis at each stage. They also perform better as fibrosis stage rises. Although SWE and STE provide 2-D stiffness visualization combined with US B-mode imaging for anatomic information, they are not superior in performance to VCTE, which provides a median value of 10 blind measurements. This may indicate that the selection of ROI in SWE and STE does not affect diagnostic performance but may affect the number of successful measurements, as areas that are avoided by SWE or STE measurements are not detected by the VCTE examiner. Regarding the inter-observer variability study, SWE and STE achieved ICCs of 0.9610 and 0.98, respectively, indicating that both SWE and STE provide excellent inter-observer agreement. With respect to the inter-device variability study, the pairs SWE−VCTE, STE−VCTE and SWE−STE achieved ICCs of 0.92, 0.88 and 0.91, respectively, indicating that there is also excellent inter-device agreement for each pair of devices. As illustrated in Figure 6, in stages F0−F3 stages, the third and fourth quartiles of STE values are a little higher than those of SWE, and the third and fourth quartiles of SWE values are higher than those of VCTE. This is also observed in the difference in cutoff values between devices, as the SWE and STE cutoffs are ∼1 kPa higher than the VCTE cutoffs in early fibrosis stages. In the literature, differences not always following the same pattern also occur between SWE and VCTE in various studies, as reported in a recently published review (Sigrist et al. 2017). An overlap between fibrosis stages defined by stiffness cutoff values of different elastographic methods is also observed in the literature and in our results. Despite the high accuracies that all methods achieve, it should be mentioned that the overlap between stiffness values of consecutive fibrosis stages is significant, as illustrated in Figure 6. Our ROC analysis involved only binary classification fibrosis stage groups (*e.g.,* F ≥ F2 is F0−F1 vs. F2−F4 groups), and therefore, the binary diagnosis estimation is aided by the lowest stages of the first group and highest stages of the second group.

In studies that have evaluated the performance of SWE, STE and VCTE, similar results have been obtained. Ren et al. (2018) obtained a similar accuracy (0.87) in STE's F ≥ F2 differentiation performance, while the corresponding accuracy for VCTE was
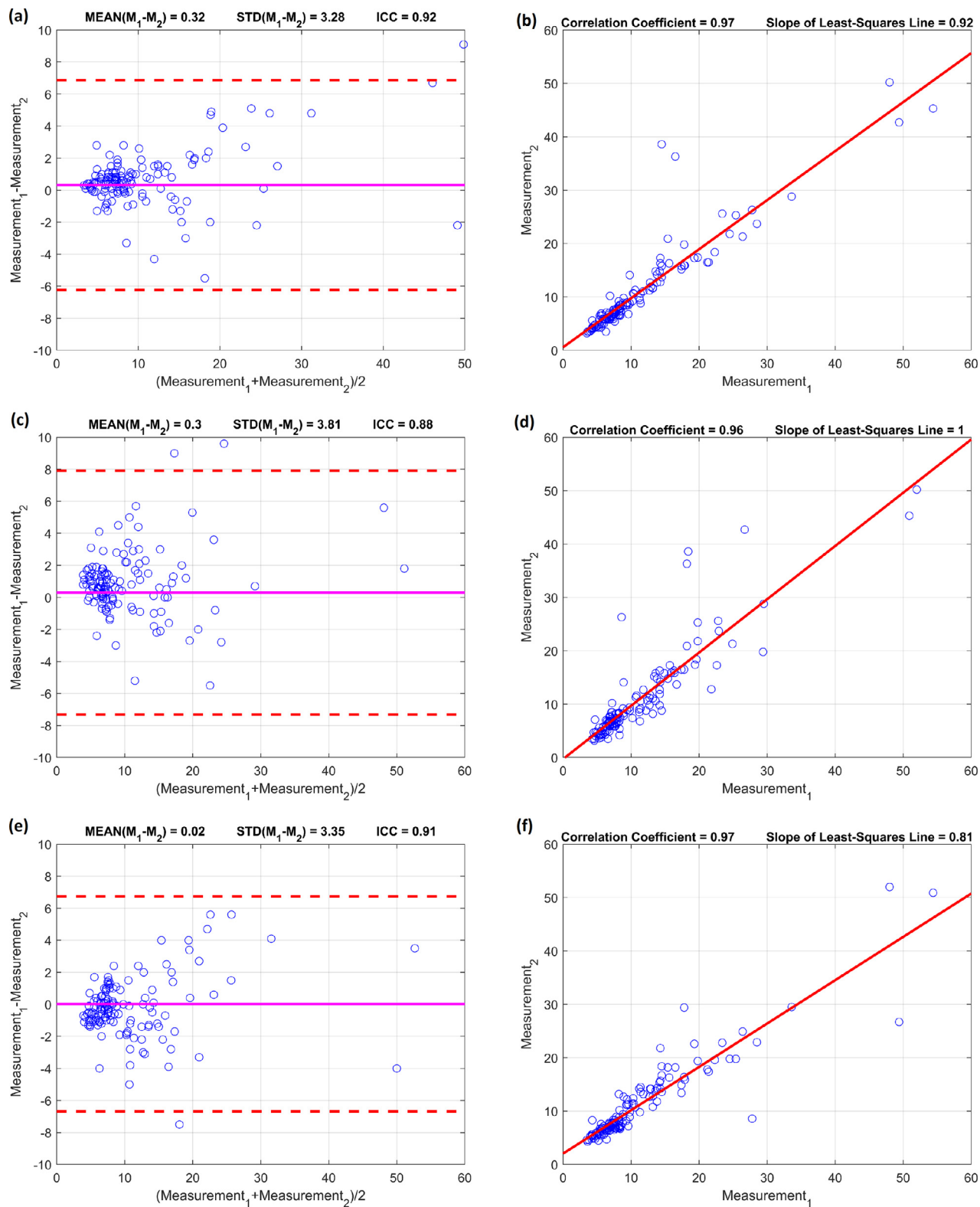
Fig. 5. (a,b) SWE−VCTE Bland−Altman (a) and least-squares line (b) plots. (c,d) STE−VCTE Bland−Altman (c) and least-squares line (d) plots. (e,f) SWE−STE Bland−Altman (e) and least-squares line (f) plots. Measurements were made to assess inter-device variability. ICC = intra-class correlation coefficient; STD = standard deviation; SWE = shear wave elastography; STE = sound touch elastography; VCTE = vibration-controlled transient elastography.
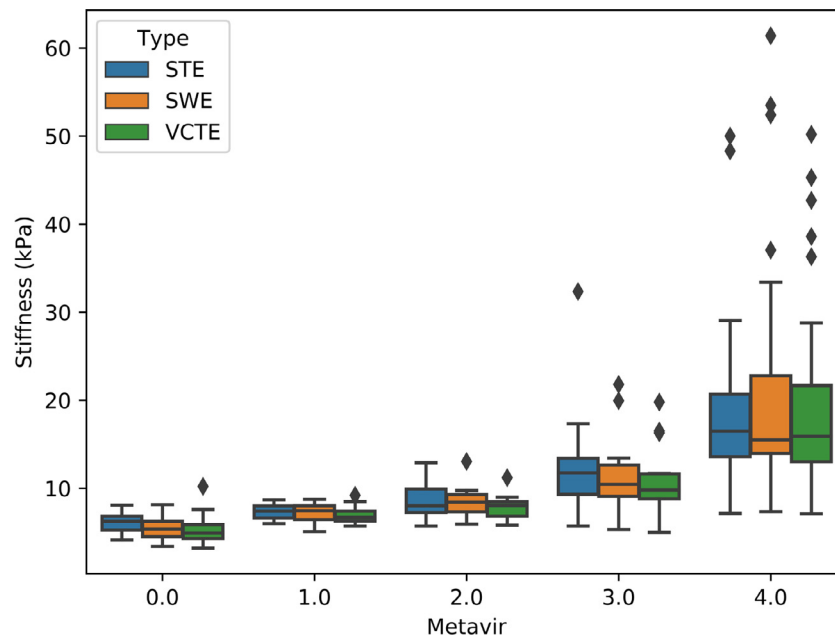
Fig. 6. Box plots of stiffness values (y-axis) for each fibrosis stage (x-axis) and ultrasound device.

significantly lower (0.648); the performance of STE in other fibrosis stage classes was not evaluated. Most other studies (Talwalkar et al. 2007; Vizzutti et al. 2009; Tsochatzis et al. 2011; Ferraioli et al. 2012, 2015; Bamber et al. 2013; Bota et al. 2013, 2015; Chung et al. 2013; Cosgrove et al. 2013; Hong et al. 2014; Sporea et al. 2014; Deffieux et al. 2015; Gerber et al. 2015; Kobayashi et al. 2015; Sigrist et al. 2017; Herrmann et al. 2018) obtained similar results for the performance of SWE and VCTE for the various fibrosis stage classes.

To the best of our knowledge, this is the first study to compare STE performance with that of known and established US elastographic techniques such as SWE from Supersonic Imagine and VCTE (Fibroscan) from Echosens in CLD assessment.

The fact that all patients underwent processing and SWE and STE examinations in a single clinic limits generalization of the results. VCTE measurements were performed at two other remote medical centers, but only one radiologist took measurements on each patient, and therefore, inter-observer analysis of VCTE measurements was not possible. The relatively small sample size did not permit an ROC analysis for each CLD subtype. Also, the sample was not equally distributed among the fibrosis stages; in particular, our F2 group consisted of only 12 patients. This may have significantly affected the calculation of cutoff values. There may exist a potential, but not probable, difference between the LB-estimated fibrosis stage of a patient and his or her stage when STE, SWE and VCTE examinations were performed. Usually, CLD progresses at a slow rate, takes many years to develop into fibrosis and, if unopposed, cirrhosis. A number of studies have reported that progression from one stage to another may take even decades (Pinzani et al. 2001; Poynard et al. 2003). To establish a desirable number of patients but minimize the possibility that a fibrosis patient's stage (estimated by LB) has progressed significantly when examined with elastographic methods and vice versa, we used an interval of 6 mo, which is arbitrary but probably safe for fibrosis stage non-progression. Our previously published studies made the same assumption (Gatos et al. 2016, 2017, 2019). Moreover, in this study, indices that are related to the reliability criteria of STE/SWE manufacturers (STE's five-star index and Aixplorer's SI) were not recorded, and therefore, factors that affect STE/SWE image quality were not analyzed. A future study can include relative metrics to investigate whether poor STE/SWE image quality metrics are related to disease or other clinical factors.

CONCLUSIONS

A study evaluating the performance of two popular US elastography methods, in comparison with STE, a relatively new method, was carried out. STE performs similarly to VCTE and SWE in terms of accuracy, and could be used as alternative to the other methods. Furthermore, all methods exhibit good inter-observer and inter-device variability provided that the examinations are performed by an expert radiologist and device-specific guidelines of the manufacturers and EFSUMB recommendations are followed. More patients should be processed to further validate STE as a new, reliable alternative US elastography method.

REFERENCES

Akkaya HE, Erden A, Kuru Oz D, Unal S, Erden I. Magnetic resonance elastography: Basic principles, technique, and clinical applications in the liver. Diagn Interv Radiol Turkey 2018;24:328–335.

Asrani SK, Devarbhavi H, Eaton J, Kamath PS. Burden of liver diseases in the world. J Hepatol 2019;70:151–171.

Bamber J, Cosgrove D, Dietrich CF, Fromageau J, Bojunga J, Calliada F, Cantisani V, Correas J-M, D'Onofrio M, Drakonaki EE, Fink M, Friedrich-Rust M, Gilja OH, Havre RF, Jenssen C, Klauser AS, Ohlinger R, Saftoiu A, Schaefer F, Sporea I, Piscaglia F. EFSUMB guidelines and recommendations on the clinical use of ultrasound elastography: Part 1. Basic principles and technology. Ultraschall Med 2013;34:169–184.

Bland JM, Altman D. Measuring agreement in method comparison studies. Stat Methods Med Res 1999;8:135–160.

Bota S, Herkner H, Sporea I, Salzl P, Sirli R, Neghina AM, Peck-Radosavljevic M. Meta-analysis: ARFI elastography versus transient elastography for the evaluation of liver fibrosis. Liver Int 2013;33:1138–1147.

Bota S, Paternostro R, Etschmaier A, Schwarzer R, Salzl P, Mandorfer M, Kienbacher C, Ferlitsch M, Reiberger T, Trauner M, Peck-Radosavljevic M, Ferlitsch A. Performance of 2-D shear wave elastography in liver fibrosis assessment compared with serologic tests and transient elastography in clinical routine. Ultrasound Med Biol 2015;41:2340–2349.

Carey E, Carey WD. Noninvasive tests for liver disease, fibrosis, and cirrhosis: Is liver biopsy obsolete? Cleve Clin J Med 2010;77:519–527.

Chung JH, Ahn HS, Kim SG, Lee YN, Kim YS, Jeong SW, Jang JY, Lee SH, Kim HS, Kim BS. The usefulness of transient elastography, acoustic-radiation-force impulse elastography, and real-time elastography for the evaluation of liver fibrosis. Clin Mol Hepatol 2013;19:156–164.

Cosgrove D, Piscaglia F, Bamber J, Bojunga J, Correas J-M, Gilja OH, Klauser AS, Sporea I, Calliada F, Cantisani V, D'Onofrio M, Drakonaki EE, Fink M, Friedrich-Rust M, Fromageau J, Havre RF, Jenssen C, Ohlinger R, Saftoiu A, Schaefer F, Dietrich CF. EFSUMB guidelines and recommendations on the clinical use of ultrasound elastography: Part 2. Clinical applications. Ultraschall Med 2013;34:238–253.

Deffieux T, Gennisson JL, Bousquet L, Corouge M, Cosconea S, Amroun D, Tripon S, Terris B, Mallet V, Sogni P, Tanter M, Pol S. Investigating liver stiffness and viscosity for fibrosis, steatosis and activity staging using shear wave elastography. J Hepatol 2015;62:317–324.

Dietrich CF, Bamber J, Berzigotti A, Bota S, Cantisani V, Castera L, Cosgrove D, Ferraioli G, Friedrich-Rust M, Gilja OH, Goertz RS, Karlas T, de Knegt R, de Ledinghen V, Piscaglia F, Procopet B, Saftoiu A, Sidhu PS, Sporea I, Thiele M. EFSUMB Guidelines and Recommendations on the Clinical Use of Liver Ultrasound Elastography, Update 2017 (long version). Ultraschall Med 2017;38:e16–e47.

Dong F, Wu H, Zhang L, Tian H, Liang W, Ye X, Liu Y, Xu J. Diagnostic performance of multimodal sound touch elastography for differentiating benign and malignant breast masses. J Ultrasound Med 2019;38:2181–2190.

Ferraioli G, Tinelli C, Dal Bello B, Zicchetti M, Filice G, Filice C. Accuracy of real-time shear wave elastography for assessing liver fibrosis in chronic hepatitis C: A pilot study. Hepatology 2012;56:2125–2133.

Ferraioli G, Filice C, Castera L, Choi BI, Sporea I, Wilson SR, Cosgrove D, Dietrich CF, Amy D, Bamber JC, Barr R, Chou YH, Ding H, Farrokh A, Friedrich-Rust M, Hall TJ, Nakashima K, Nightingale KR, Palmeri ML, Schafer F, Shiina T, Suzuki S, Kudo M. WFUMB guidelines and recommendations for clinical use of ultrasound elastography: Part 3. Liver. Ultrasound Med Biol 2015;41:1161–1179.

Ferraioli G, Wong VWS, Castera L, Berzigotti A, Sporea I, Dietrich CF, Choi BI, Wilson SR, Kudo M, Barr RG. Liver Ultrasound Elastography: An Update to the World Federation for Ultrasound in Medicine and Biology Guidelines and Recommendations. Ultrasound Med Biol 2018;44:2419–2440.

Friedman LS, Martin P. Handbook of liver disease. 4th edition Philadelphia: Elsevier; 2017.

Frulio N, Trillaud H. Ultrasound elastography in liver. Diagn Interv Imaging 2013;94:515–534.

Gatos I, Tsantis S, Spiliopoulos S, Karnabatidis D, Theotokas I, Zoumpoulis P, Loupas T, Hazle JD, Kagadis GC. A new computer aided diagnosis system for evaluation of chronic liver disease with ultrasound shear wave elastography imaging. Med Phys 2016;43:1428–1436.

Gatos I, Tsantis S, Spiliopoulos S, Karnabatidis D, Theotokas I, Zoumpoulis P, Loupas T, Hazle JD, Kagadis GC. A machine-learning algorithm toward color analysis for chronic liver disease classification, employing ultrasound shear wave elastography. Ultrasound Med Biol 2017;43:1797–1810.

Gatos I, Tsantis S, Spiliopoulos S, Karnabatidis D, Theotokas I, Zoumpoulis P, Loupas T, Hazle JD, Kagadis GC. Temporal stability assessment in shear wave elasticity images validated by deep learning neural network for chronic liver disease fibrosis stage assessment. Med Phys 2019;46:2298–2309.

Gerber L, Kasper D, Fitting D, Knop V, Vermehren A, Sprinzl K, Hansmann ML, Herrmann E, Bojunga J, Albert J, Sarrazin C, Zeuzem S, Friedrich-Rust M. Assessment of liver fibrosis with 2-D shear wave elastography in comparison to transient elastography and acoustic radiation force impulse imaging in patients with chronic liver disease. Ultrasound Med Biol 2015;41:2350–2359.

Gilmore IT, Burroughs A, Murray-Lyon IM, Williams R, Jenkins D, Hopkins A. Indications, methods, and outcomes of percutaneous liver biopsy in England and Wales: An audit by the British Society of Gastroenterology and the Royal College of Physicians of London. Gut 1995;36:437–441.

Giorgio A, Amoroso P, Lettieri G, Fico P, de Stefano G, Finelli L, Scala V, Tarantino L, Pierri P, Pesce G. Cirrhosis: Value of caudate to right lobe ratio in diagnosis with US. Radiology 1986;161:443–445.

Goodman ZD. Grading and staging systems for inflammation and fibrosis in chronic liver diseases. J Hepatol 2007;47:598–607.

Gress VS, Glawion EN, Schmidberger J, Kratzer W. Comparison of liver shear wave elastography measurements using Siemens Acuson S3000, GE LOGIQ E9, Philips EPIQ7 and Toshiba Aplio 500 (Software Versions 5.0 and 6.0) in healthy volunteers. Ultraschall Med 2019;40:504–512.

Harbin WP, Robert NJ, Ferrucci JTJ. Diagnosis of cirrhosis based on regional changes in hepatic morphology: A radiological and pathological analysis. Radiology 1980;135:273–283.

Herrmann E, de Ledinghen V, Cassinotto C, Chu WCW, Leung VYF, Ferraioli G, Filice C, Castera L, Vilgrain V, Ronot M, Dumortier J, Guibal A, Pol S, Trebicka J, Jansen C, Strassburg C, Zheng R, Zheng J, Francque S, Vanwolleghem T, Vonghia L, Manesis EK, Zoumpoulis P, Sporea I, Thiele M, Krag A, Cohen-Bacrie C, Criton A, Gay J, Deffieux T, Friedrich-Rust M. Assessment of biopsy-proven liver fibrosis by two-dimensional shear wave elastography: An individual patient data-based meta-analysis. Hepatology 2018;67:260–272.

Hong H, Li J, Jin Y, Li Q, Li W, Wu J, Huang Z. Performance of real-time elastography for the staging of hepatic fibrosis: A meta-analysis. PLoS One 2014;9 e115702 −e115702.

Huwart L, Sempoux C, Vicaut E, Salameh N, Annet L, Danse E, Peeters F, ter Beek LC, Rahier J, Sinkus R, Horsmans Y, Van Beers BE. Magnetic resonance elastography for the noninvasive staging of liver fibrosis. Gastroenterology 2008;135:32–40.

Kobayashi K, Nakao H, Nishiyama T, Lin Y, Kikuchi S, Kobayashi Y, Yamamoto T, Ishii N, Ohashi T, Satoh K, Nakade Y, Ito K, Yoneda M. Diagnostic accuracy of real-time tissue elastography for the staging of liver fibrosis: A meta-analysis. Eur Radiol 2015;25:230–238.

Lasko TA, Bhagwat JG, Zou KH, Ohno-Machado L. The use of receiver operating characteristic curves in biomedical informatics. J Biomed Inform 2005;38:404–415.

Li RK, Ren XP, Yan FH, Qiang JW, Lin HM, Wang T, Zhao HF, Chen WB. Liver fibrosis detection and staging: A comparative study of T1 ρ MR imaging and 2 D real-time shear-wave elastography. Abdom Radiol 2018;43:1713–1722.

Li SS. Sound touch elastography: A new solution for ultrasound elastography. White Paper, Shenzhen: Mindray Bio-Medical Electronics Co. Ltd; 2015.

Martínez SM, Crespo G, Navasa M, Forns X. Noninvasive assessment of liver fibrosis. Hepatology 2011;53:325–335.

Parola M, Pinzani M. Liver fibrosis: Pathophysiology, pathogenetic targets and clinical issues. Mol Aspects Med 2019;65:37–55.

Pinzani M, Romanelli RG, Magli S. Progression of fibrosis in chronic liver diseases: Time to tally the score. J Hepatol 2001;34:764–767.

Poynard T, Mathurin P, Lai CL, Guyader D, Poupon R, Tainturier MH, Myers RP, Muntenau M, Ratziu V, Manns M, Vogel A, Capron F, Chedid A, Bedossa P. A comparison of fibrosis progression in chronic liver diseases. J Hepatol 2003;38:257–265.

Ren X, Xia S, Ni Z, Zhan W, Zhou J. Analysis of three ultrasound elastography techniques for grading liver fibrosis in patients with chronic hepatitis B. Radiol Med 2018;123:735–741.

Romero-Gómez M, Gómez-González E, Madrazo A, Vera-Valencia M, Rodrigo L, Pérez-Alvarez R, Pérez-López R, Castellano-Megias VM, Nevado-Santos M, Alcón JC, Solá R, Pérez-Moreno JM, Navarro JM, Andrade RJ, Salmerón J, Fernández-López M, Aznar R, Diago M. Optical analysis of computed tomography images of the liver predicts fibrosis stage and distribution in chronic hepatitis C. Hepatology 2008;47:810–816.

Sanford NL, Walsh P, Matis C, Baddeley H, Powell LW. Is ultrasonography useful in the assessment of diffuse parenchymal liver disease? Gastroenterology 1985;89:186–191.

Sigrist RMS, Liau J, Kaffas AEl, Chammas MC, Willmann JK. Ultrasound elastography: Review of techniques and clinical applications. Theranostics 2017;7:1303–1329.

Sporea I, Bota S, Gradinaru-Tascau O, Sirli R, Popescu A, Jurchis A. Which are the cut-off values of 2D-shear wave elastography (2D-SWE) liver stiffness measurements predicting different stages of liver fibrosis, considering transient elastography (TE) as the reference method? Eur J Radiol 2014;83:e118–e122.

Talwalkar JA, Kurtz DM, Schoenleber SJ, West CP, Montori VM. Ultrasound-based transient elastography for the detection of hepatic fibrosis: Systematic review and meta-analysis. Clin Gastroenterol Hepatol 2007;5:1214–1220.

Tsochatzis EA, Gurusamy KS, Ntaoula S, Cholongitas E, Davidson BR, Burroughs AK. Elastography for the diagnosis of severity of fibrosis in chronic liver disease: A meta-analysis of diagnostic accuracy. J Hepatol 2011;54:650–659.

Vizzutti F, Arena U, Marra F, Pinzani M. Elastography for the non-invasive assessment of liver disease: Limitations and future developments. Gut 2009;58:157–160.

Zhang L, Ding Z, Dong F, Wu H, Liang W, Tian H, Ye X, Luo H, Xu J. Diagnostic performance of multiple sound touch elastography for differentiating benign and malignant thyroid nodules. Front Pharmacol 2018;9:1359.